Journal of Applied Physics

Conductivity relaxation and photocurrent generation in reduced graphene oxide-poly(9,9'-dioctyl-fluorene-co-bithiophene) composite with application in temperature sensing

Cite as: J. Appl. Phys. **125**, 085104 (2019); https://doi.org/10.1063/1.5087968
Submitted: 07 January 2019 . Accepted: 02 February 2019 . Published Online: 26 February 2019

Poulomi Das, Koushik Chakraborty, Arvind Pan, Surajit Ghosh, and Tanusri Pal

AIP Publishing

Journal of Applied Physics ARTICLE scitation.org/journal/jap

Conductivity relaxation and photocurrent generation in reduced graphene oxide-poly (9,9′-dioctyl-fluorene-co-bithiophene) composite with application in temperature sensing

Cite as: J. Appl. Phys. **125**, 085104 (2019); doi: 10.1063/1.5087968
Submitted: 7 January 2019 · Accepted: 2 February 2019 ·
Published Online: 26 February 2019

Poulomi Das,[1] Koushik Chakraborty,[2] Arvind Pan,[3] Surajit Ghosh,[2] and Tanusri Pal[1,a)]

AFFILIATIONS

[1]Department of Physics, Midnapore College, Midnapore, West Bengal 721101, India
[2]Department of Physics & Technophysics, Vidyasagar University, Midnapore, West Bengal 721102, India
[3]Department of Physics, Vivekananda College, University of Calcutta, Thakurpukur, Kolkata, West Bengal 700063, India

[a)]**Author to whom correspondence should be addressed:** tanusri.pal@gmail.com

ABSTRACT

The electrical transport properties and photocurrent generation in a reduced graphene oxide-poly(9,9′-dioctyl-fluorene-co-bithiophene) (RGO-F8T2) composite were investigated. The semiconducting nature of the RGO-F8T2 composite was jointly demonstrated by dc and ac conductivity measurements. The dc conductivity obtained from both dc and ac measurements follows the Arrhenius relationship with the activation energy of the order of 80 meV. The RGO-F8T2 composite also showed excellent temperature sensing properties. The temperature coefficient of resistance was compared to commercially available Platinum, Polysilicon, and Germanium temperature sensor. The conductivity relaxation mechanism in the RGO-F8T2 composite depicted the mechanism behind ac conduction. This was due to phonon assisted tunneling between the defect states. The density of states at the Fermi level increases by one order of magnitude for the temperature change of 301 to 433 K. The scaling of conductivity isotherms established the occurrence of intramolecular energy transfer from disordered to ordered chain segments or both in the composite. The photocurrent generation in the RGO-F8T2 composite thin film under simulated solar light illumination was also studied. Here, a linear variation of the photosensitivity with the variation of the incident light intensity was observed.

I. INTRODUCTION

Betting on organic and polymer semiconductors by device physics researchers is the obvious choice nowadays.[1] The motive behind this is simply the increased necessity of flexible and lightweight devices in our daily lives. The solution processable organic/inorganic hybrid systems not only meet this requirement but also pave a way to cost effective mass production by using high throughput and large area printing by circumventing the conventional processes like photolithographic printing.[2–5] Of course, there exist quite a few operational prototype polymer semiconductors.[6] But those need further improvement in terms of device performance and lifetime, when compared with the traditional inorganic semiconductor, keeping in view of technological competitiveness. In order to meet these ends, one needs to have a deeper understanding of the physics behind the transport and conductivity relaxation mechanism.

In recent times, copolymers based on fluorene have emerged as potential semiconductor optoelectronic materials for Photo Voltaic (PV) application. High carrier mobility with easy processability and efficient visible light absorbance capacity makes them an attractive candidate in the optoelectronic device applications. The physical properties of this class of materials can be engineered by assembling various copolymers. Among them, poly(9,9′-dioctyl-fluorine-co-bithiophene) (F8T2) has become a common name for the

Organic Field Effect Transistor (OFET)[7,8] over the last few years. Until now, the studies on transport of F8T2 had concentrated themselves on the device characteristics such as transfer characteristics and carrier mobilities in the conventional source drain configuration.[9–11]

We, therefore, had confined our focus of study to the complementary approach of electrical transport on the solution processed F8T2 on reduced graphene oxide (RGO).[12–14] This study will not only shed light on the transport and conductivity relaxation in terms of the Quantum Mechanical Tunneling model of disordered solids but also provide us with some very important physical parameters like the density of states at Fermi Level [$N(E_F)$] for different temperatures.

The variation of resistance with temperature tempts one to explore the applicability as a temperature sensor. It has been found that the temperature coefficient of resistance (TCR) of the RGO-F8T2 composite is comparable to many available commercial temperature sensors.

Hence, in this work, we present the synthesis, characterization, electrical conductivity, and temperature sensing activity of the RGO-F8T2 composite. The composite was synthesized by the reduction of GO in the presence of F8T2, using hydrazine hydrate as a reducing agent. The crystallinity and reduction efficiency was confirmed by XRD, XPS, FTIR, and Raman study. The electronic interaction was established with the help of UV-Vis absorption and PL measurement. The AC conductivity was measured within a wide range of temperature and frequency. In addition to that the visible light photo current generation using a thin film photodetector was also investigated. The present study offers several new insights into the electrical conduction mechanism in RGO based composite materials. Besides this, our findings establish the RGO-F8T2 composite as a promising temperature sensor and a potential optoelectronic material for various prospective applications.

II. EXPERIMENTAL PROCEDURE

A. Materials

Graphite, potassium persulfate ($K_2S_2O_8$), phosphorus pentoxide (P_2O_5), sodium nitrate ($NaNO_3$), poly[9,9′-dioctylfluorene-co-bithiophene] (F8T2), hydrazine hydrate (N_2H_4), and N,N-dimethylformamide (DMF) were purchased from Sigma-Aldrich. Potassium permanganate ($KMnO_4$), sulfuric acid (H_2SO_4), hydrogen peroxide (H_2O_2), hydrochloric acid (HCl), and tetrahydrofuran (THF) were purchased from Merck, India. All chemicals were used as received.

B. Synthesis of RGO-F8T2 composites

Graphene oxide (GO) was synthesized by the modified Hummers' method from graphite powder purchased from Sigma-Aldrich, in the presence of $K_2S_2O_8$ (1 g), P_2O_5 (1 g), $NaNO_3$ (0.1 g), $KMnO_4$ (0.6 g), 98% H_2SO_4 (20 ml), and H_2O_2 (12 ml, 3 wt. %) under stirring at 80 °C.[15] The mixture was then filtered and washed with double distilled (DD) water for several times and dried at 60 °C for 24 h. Finally, the brownish graphite oxide (GO) powder was obtained. A homogeneous solution of GO (2 mg) in DMF (5 ml) was formed by ultrasonication. Initially, a homogeneous lemon yellow F8T2 (1 mg) solution was prepared by dissolving it in 5 ml THF under continuous stirring. Then, the F8T2 solution was heated up to 85 °C in an oil bath under the stirred condition for evaporation of THF. In this period, 5 ml of DMF was added dropwise into the F8T2 solution towards replacing THF by DMF solvent. In the next step, the as-prepared F8T2 and GO solution (1:2) was added under stirring, and finally, reduction was done by hydrazine hydrate (1 μl/10 mg GO) at 80 °C for 12 h in an oil bath. The colour of the solution changed to dark greenish yellow, and a RGO-F8T2 composite was formed.

C. Material characterization

The powder X-ray diffraction (XRD) patterns of as-prepared GO, F8T2, RGO, and RGO-F8T2 composites were recorded ($2\theta = 2°–70°$) by a Rigaku-Miniflex X-ray diffractometer with CuK_α radiation ($\lambda = 0.15418$ nm), operated at 30 kV and 10 mA. The Fourier transform infrared (FTIR) transmittance was recorded with a Perkin Elmer Spectrum 100 spectrophotometer. The reduction of GO and the formation of the RGO-F8T2 composite were confirmed by X-ray photoelectron spectroscopy (XPS) study, and they were carried out with an X-ray photoelectron spectroscope (ULVAC-PHI, 5000 Versa Probe II spectrometer) with the AlK_α (1486.6 eV, 25 W, and 15 kV) source. Survey scans were recorded over wide range from 0 to 1200 eV. Peak deconvolution was carried out by using Gaussian components. Absorbance spectra of the prepared samples were recorded by a UV-Visible Spectrophotometer (Shimadzu UV-1700), and steady state photoluminescence (PL) of the F8T2 and RGO-F8T2 composites was analyzed with a fluorescence spectrophotometer (Perkin Elmer LS 55). The bandgap energy (E_g) of F8T2 was calculated from the absorbance spectrum with the help of the relation $\alpha h\nu = A\ (h\nu - E_g)^{1/2}$, where α, $h\nu$, and A are absorption co-efficient, photon energy, and material constant, respectively.

D. Electrical conductivity measurement

For electrical conductivity measurement, a pellet (thickness 0.04 cm and area 0.5 cm^2) was formed at room temperature under 5 ton/cm^2 pressure. Current–Voltage (I-V) measurement of the sample was carried out using a Keithley 2612A sourcemeter in the temperature range of 301 to 433 K. The frequency dependent capacitance [$C(w)$] and conductance [$G(w)$] of the RGO-F8T2 pellet was measured by using an Agilent E4980A LCR meter in the frequency range 20 Hz–2 MHz and temperature range 301 K to 433 K. The real (Z') and imaginary (Z'') parts of complex impedance were found out from the equations

$$Z' = G(\omega)/[G^2(\omega) + \omega^2\{C(\omega) - C_0\}^2], \quad (1)$$

$$Z'' = [C(\omega) - C_0]\omega/[G^2(\omega) + \omega^2\{C(\omega) - C_0\}^2], \quad (2)$$

where C_0 is the null temperature. The real part of conductivity [$\sigma'(\omega)$] was determined as $\sigma'(\omega) = G(\omega)lA^{-1}$, where $G(\omega)$ is the

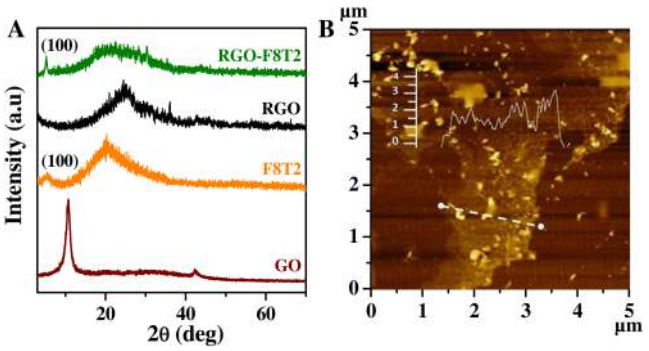

FIG. 1. (a) XRD patterns of the GO, F8T2, RGO, and RGO-F8T2 composites. (b) AFM image of RGO-F8T2 composite films on a silicon wafer.

conductance at frequency domain ω, and l and A are thickness and area of the RGO-F8T2 pallet, respectively.

E. Temperature sensing study

In order to study the temperature sensing activity of the RGO-F8T2 composite, the resistance of the composite (in pellet form) was determined from the I-V characteristic curves. Data were recorded by a Keithley 2612A sourcemeter in the temperature range of 301 to 433 K. The TCR was calculated from the temperature dependent resistance of the RGO-F8T2 composite.

F. Device fabrication and photocurrent measurements

To study the photocurrent generation, a thin film photodetector based on the RGO-F8T2 composite was fabricated. A solar light simulator (Oriel 67005, Newport, AM 1.5) was employed as the illuminated light source. Thin film was prepared by the simple drop casting method on a pre-cleaned glass substrate and was annealed on a hot plate for better formation of the film. A pair of parallel electrodes was painted using conducting silver paste (Ted Pella). To study the photocurrent generation in the ambient condition, a Keithley 2612A sourcemeter was engaged, and the data were recorded by LabTracer 2.0 software. The incident light power varied from 100 to 160 mW cm^{-2}, and the power was measured using an optical power meter (Newport 843-R). The photocurrent (I_{Ph}) was calculated using the equation $I_{Ph} = I_L - I_D$, where I_L and I_D represent the current under illumination and darkness, respectively.

III. RESULTS AND DISCUSSION

The X-ray diffraction pattern of GO, F8T2, RGO, and RGO-F8T2 composites has been presented in Fig. 1(a). A sharp and intense peak centered at $2\theta = 10.7°$ with interplanner spacing of 0.83 nm indicates the incorporation of oxygen-containing groups into the carbon layers due to the oxidation of graphite and the formation of GO.[16] In the diffraction pattern of F8T2, a peak at 5.2° corresponding to (100) plane and a hump at 20.3° are displayed clearly. In RGO-F8T2 diffraction pattern, the peak for GO at 10.7° completely disappeared and the peak attributed to F8T2 remains at the same position while the hump at 20.3° becomes broadened due to additional hump arising from RGO at 24.8°. It is also observed that the peak of F8T2 becomes sharp in the composite due to the mild thermal annealing at the time of composite synthesis. In order to have an insight into the surface topology of individual layer, AFM imaging of the spin-coated RGO-F8T2 composite was performed. As observed in Fig. 1(b), the average thickness of the RGO-F8T2 sheet is ~2.28 nm which is higher than a RGO monolayer (~1 nm), indicating the attachment of F8T2 on the basal plan of RGO via π-π interaction. The reduction of GO and the formation of RGO-F8T2 were confirmed by the FTIR study. Figure 2(a) compares the FTIR spectrum of the GO, F8T2, RGO, and RGO-F8T2 composites. In the FTIR spectra of GO, the absorption band for skeletal vibrations of non-oxidized graphitic domains (C=C stretching) and the peaks for the stretching vibration of −C=O, C−O, and C−O−C are observed clearly.[17,18] The FTIR

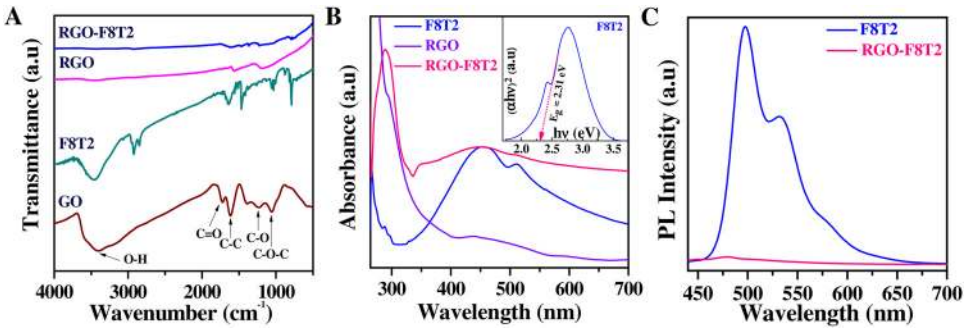

FIG. 2. (a) FTIR spectra of the GO, F8T2, RGO, and RGO-F8T2 composites. (b) Optical absorption spectra of the F8T2, RGO, and RGO–F8T2 composites. Plot of $(\alpha h\nu)^2$ vs photon energy of F8T2 is shown in the inset. (c) Photoluminescence spectra of the F8T2 and the RGO-F8T2 composites.

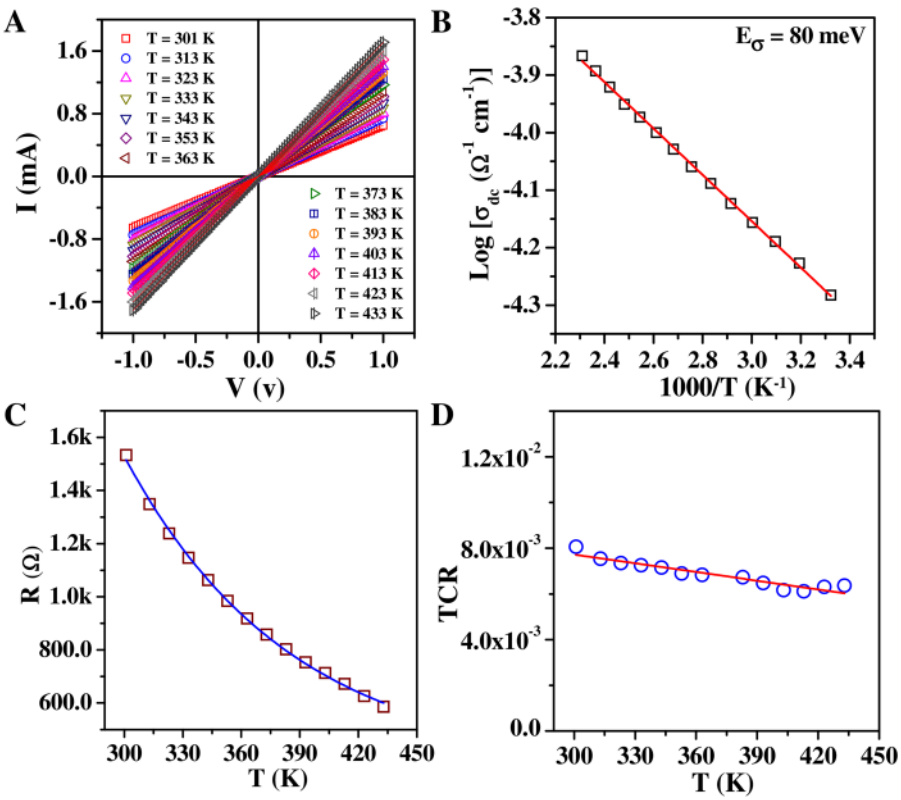

FIG. 3. (a) I-V characteristics of the RGO-F8T2 composite pellet. (b) The Arrhenius behaviour of dc conductivity with its straight line fit. Variation of (c) resistance and (d) TCR with temperature of the RGO-F8T2 composite.

spectrum of controlled-F8T2 is similar to the other reported work.[19] In the RGO-F8T2 spectrum, the absorption peaks oriented with oxygen containing functional groups have almost disappeared and another band is observed which confirms C=C skeletal vibration of graphene sheets. The electronic interaction among F8T2 and RGO was investigated by UV-Vis absorption study and presented in Fig. 2(a). The sharp absorbance peak at 456 nm with a shoulder peak at 511 nm is clearly observed in the UV-Vis spectrum of controlled-F8T2, which is very close to the previous reported value.[19] In RGO-F8T2, all the peaks associated with F8T2 are present and the peaks broaden, revealing the formation of the RGO-F8T2 hybrid. A new peak at 289 nm ascribed as the π-plasmon of the graphitic structure is also present in RGO-F8T2. In addition to that in the presence of RGO, the absorbance capacity of the composite increases in 300–600 nm region in contrast to the controlled F8T2, which is due to the augmentation of absorption contribution from RGO and F8T2. Also, the scattering effect of RGO may have some roles on the absorption property of the composite. The enhancement of absorption in the visible region is advantageous for the photocurrent generation. In order to explore the photo induced charge transformation between F8T2 and RGO, steady-state PL in the DMF solvent at room temperature was performed and shown in Fig. 2(c). F8T2 gives an emission maximum at 500 nm with shoulder humps at 532 nm and 573 nm. A dramatically quenching (95%) in PL is observed in the emission spectrum of RGO-F8T2 in the identical experimental condition. Significant quenching of PL is evident for photo-induced charge transfer through the interface of F8T2 and RGO. The interaction between F8T2 and RGO and the reduction of GO were further confirmed from XPS spectra.

Figure 3(a) shows I–V characteristics of the pellet samples of the RGO-F8T2 composite. The corresponding dc conductivity was computed and plotted with inverse temperature in Fig. 3(b). The nature of the plots confirmed the semiconducting behavior of the RGO-F8T2 composite. The activation energy (80 meV) was computed from the slope of the graphs, and the valued agreed with the data present in the literature,[20] thereby confirming the presence of the F8T2 layer on RGO. The temperature dependence of resistance of the pellet sample is presented in Fig. 3(c). The solid line is the exponential fit of the experimental data. This line depicts the exponential decay of resistance with temperature. This leads

to a negative TCR, which can be expressed as follows:

$$\mathrm{TCR} = \ln\left(\frac{R}{R_s}\right)/(T_s - T), \tag{3}$$

where R is the resistance corresponding to temperature T and R_s is the resistance at a particular temperature T_s. The variation of TCR with temperature is shown in Fig. 3(d), where the solid line is the linear fit. The TCR of the RGO-F8T2 composite varies linearly from 7×10^{-3} to $8\times10^{-3}\,K^{-1}$ within our investigated temperature range. It should be mentioned here that the TCR of platinum, which is considered as a potential temperature sensor due to its high TCR and time stability, is $3.9\times10^{-3}\,K^{-1}$.[21] Our findings establish the RGO-F8T2 composite as a reliable temperature sensor with a negative temperature coefficient of resistance (nTCR), which is more sensitive compared to Platinum, Polysilicon, and Germanium, commercially available temperature sensors with high TCR.[21]

In order to provide a complete picture from the point of view of impedance spectroscopy, we provide the Cole–Cole plot of the RGO-F8T2 composite in Fig. 4(a) for all the temperature range. This is a plot of the real part of the impedance Z′ versus the imaginary part of the impedance Z″. One can conclude a Debye type of relaxation from the semicircular arcs.[22] The arcs were extrapolated to the real part of the impedance axis to obtain the dc conductivity. This was done to verify the value of activation energy, which was obtained from the plot of dc conductivity obtained from Cole–Cole plot with the inverse temperature shown in Fig. 4(b).

The conductivity relaxation mechanism was explored by plotting the real part of the complex conductivity (σ') as a function of angular frequency (ω) of the applied electric field for the same temperature range at which the dc measurements were performed [Fig. 4(c)]. These conductivity spectra showed the presence of a crossover frequency (ω_c), below which the conductivity remained frequency independent and above which it became frequency dependent. This characteristic was

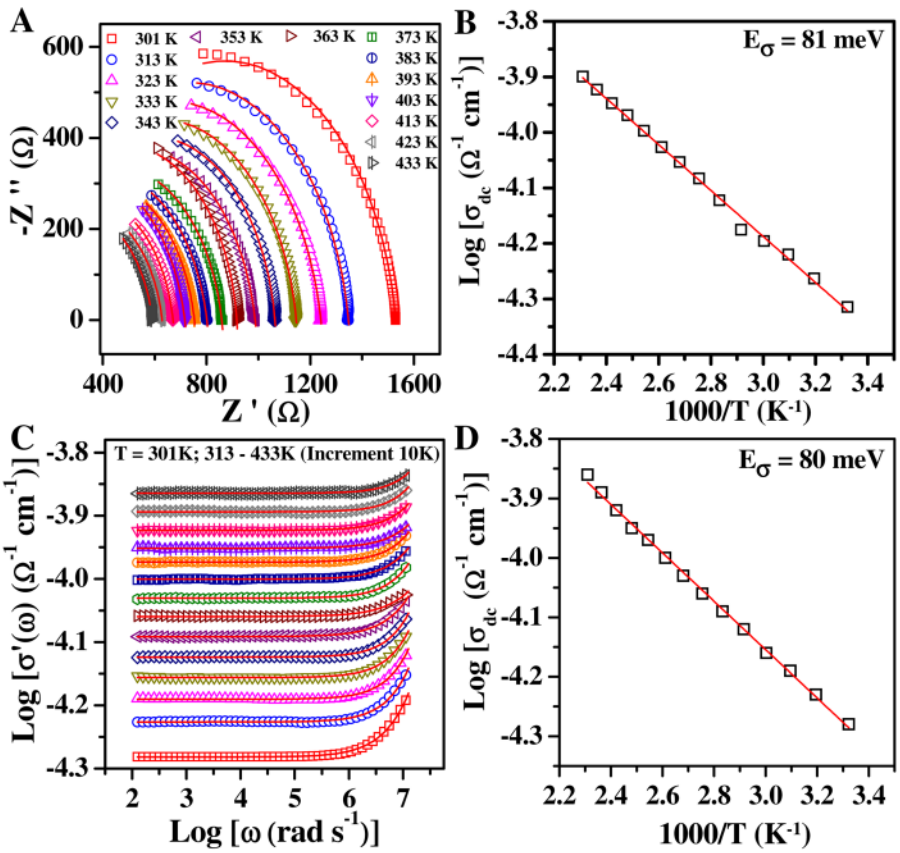

FIG. 4. (a) Z′ vs Z″ curve with equation of circle fits of the RGO-F8T2 composite pellet. (b) The Arrhenius behaviour of dc conductivity with its straight line fit. (c) The frequency spectra of the real conductivity σ′(ω) for different temperatures. The solid lines are the best fits to Eq. (5). (d) The Arrhenius behaviour of dc conductivity with its straight line fit.

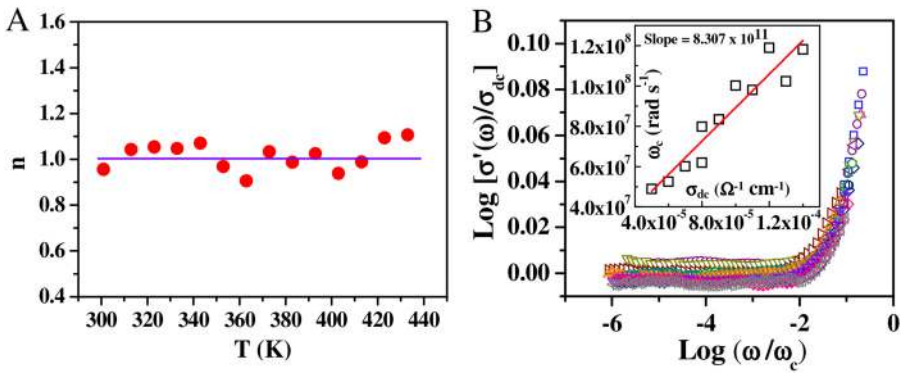

FIG. 5. (a) Variation of n with temperature. (b) Plot of log $[\sigma'(\omega)/\sigma_{dc}]$ versus log $[\omega/\omega_c]$ at different temperatures.

explained in the literature for a variety of solids.[23–29] The expression for the conductivity is given by the relation

$$\sigma'(\omega) = \sigma_{dc} + \sigma_{ac} = \sigma_{dc} + A\omega^n, \quad (4)$$

where A is a constant, which depends on the property of the material. The expression was further modified by Almond and West[29–32] to incorporate the crossover frequency (ω_c). According to the Almond West formalism, the equation for conductivity became

$$\sigma'(\omega) = \sigma_{dc}\left[1 + \frac{\omega}{\omega_c}\right]^n. \quad (5)$$

The data obtained for the RGO-F8T2 composite were fitted to the above equation. The values of σ_{dc}, ω_c, and n were obtained from the least square fits of the conductivity spectra. The dc conductivity obtained from these plots was again plotted with inverse temperature, and the activation energy was found [Fig. 4(d)] to be exactly the same as obtained from I-V measurements. The values of the frequency exponent n obtained from the fits were plotted as a function of temperature in Fig. 5(a). It was observed that the value of n is of the order of unity. Moreover, the values of n were weakly temperature dependent in the range of measurement (301 K–433 K). Hence, it can be inferred that the ac conductivity mechanism is due to phonon assisted tunneling between the defect states. In the literature, this is called the Quantum Mechanical Tunneling in disordered solids and the ac conductivity took the functional form[24,25,29,33–35]

$$\sigma_{ac} = ce^2k_BTa[N(E_F)]^2\omega R_\omega^4, \quad (6)$$

where c is a constant, e is the electronic charge, a is the inverse of localization length (α^{-1}), $N(E_F)$ is the density of states (DOS) at the Fermi level, and R_ω is the tunneling distance at a particular frequency. The Quantum Mechanical Tunneling Model was applied to the ac conductivity data of the composite to determine the relevant physical parameters. In order to achieve this, the localization length was assumed to be 16 Å as this was the value of periodicity obtained from the X ray scans in a wide temperature range.[36] The values of physical parameters related to the transport are presented in Table I. It can be observed that an order of magnitude change of $N(E_F)$ has occurred as one goes from 301 K to 433 K.

The values of crossover frequency obtained from the fit were plotted with dc conductivity [Fig. 5(b), inset], and they were found to obey the Barton Nakajima Namikawa relation.[29] This confirmed that the conductivity is due to the diffusion of the charge carriers across the networks. One can think of scaling the conductivity spectra from the view of the nature of the curves presented in Fig. 5(b). The equation of the Almond West formalism also predicted the time temperature superposition principle. This principle is a consequence of the fact that the conductivity relaxation phenomenon will be independent of time and temperature. Keeping the principle in mind, we scaled the conductivity axis with σ_{dc}, the dc conductivity, and the frequency axis with ω_c, the crossover frequency. But, to our surprise, we could not superpose the spectra for all the temperature range as shown in Fig. 5(b). The reason attributed was the conformational relaxation occurring in F8T2 in this temperature range.[21] This was due to the intra-molecular energy transfer from disordered to ordered chain segments or both.[37,38] Although the dependence of scaling of conductivity spectra on the structure was well documented and reported for inorganic glasses,[39] yet

TABLE I. Values of the physical quantities related to transport as obtained from the nonlinear curve fitting of the existing theoretical models.

Temperature (K)	σ_{dc} (Ω^{-1} cm^{-1})	ω_c (rad s^{-1})	$N(E_F)$ at 1 MHz (eV^{-1} cm^{-3})
301	5.23×10^{-5}	4.89×10^{7}	3.8×10^{19}
433	1.37×10^{-4}	1.18×10^{8}	2.86×10^{20}

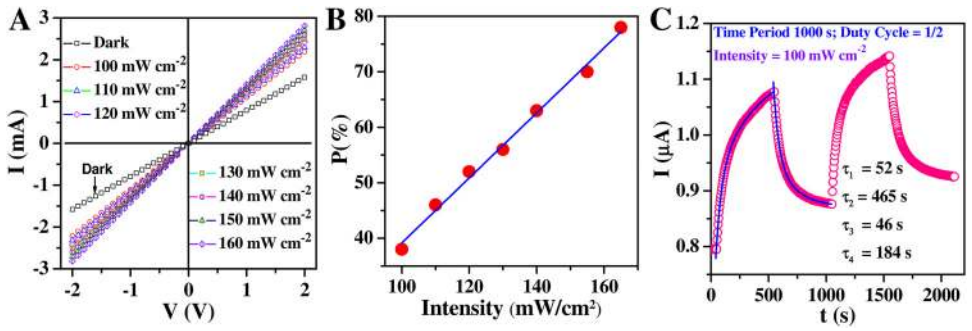

FIG. 6. I–V characteristics for a RGO–F8T2 composite thin film device under the dark condition and under different illumination intensities. (b) The variation of photosensitivity with illuminated intensity. (c) Current versus time for two consecutive cycles as the light was turned on and off.

there were no such reports for the case of organic semiconducting polymers. Thus, this study provided a generalization of the fact that—if there occurs a certain structural reconfiguration, be it due to temperature or due to concentration, then there would be a signature on the scaled conductivity spectra.

Recently, RGO based composite materials have received significant attention as an active material for the development of cost effective and high performance optoelectronic device application.[40–43] The UV-vis and PL studies jointly authenticate RGO-F8T2 as a promising optoelectronic material. The photocurrent measurement was performed by fabricating a thin film photodetector. All the I-V curves [Fig. 6(a)] show ohmic conduction for both dark and illumination conditions with the measurable bias voltage (–1 V to 1 V). A linear variation of photosensitivity (P), the ratio of photocurrent to dark current,[44,45] with the illuminated optical power, is observed and is presented in Fig. 6(b). The linear variation of the photosensitivity is advantageous towards the device application. A similar relationship between P and incident optical power was also observed in several carbon nanotubes and RGO-based compounds.[46–48] 79% photosensitivity at 160 mw/cm^2 was observed in the RGO-F8T2 based device. The photocurrent generation can be explained by the excitonic picture. Under the illuminated condition, excitons are formed in F8T2, which subsequently dissociate at the interface of RGO-F8T2 and create electron and hole carriers. The samples showed high photosensitivity as the presence of RGO resists the recombination tendency of the photo-generated carriers in F8T2 by channelizing the electron through the RGO mat.

The dynamical photoresponse of RGO-F8T2 thin films under 100 mW/cm^2 optical power was investigated and is presented in Fig. 6(c). The illuminated source was chopped by a mechanical chopper with a time interval of 500 s. When the light was turned on, initially, the device current grew very rapidly, and then slowly it got saturated at the value of 1.14 μA. After turning off the light, the current started to decrease and reached to ~0.88 μA near to its initial dark value (0.79 μA). The photocurrent of the film for growth (ON) and decay (OFF) can be described by

$$I(t) = I_{dark} + A\left\{1 - e^{\frac{-(t-t_0)}{\tau_1}}\right\} + B\left\{1 - e^{\frac{-(t-t_0)}{\tau_2}}\right\} \text{ for growth,} \quad (7)$$

$$I(t) = I_{dark} + Ce^{\frac{-(t-t_0)}{\tau_3}} + De^{\frac{-(t-t_0)}{\tau_4}} \text{ for decay,} \quad (8)$$

where τ_1, τ_2, τ_3, and τ_4 are the photoresponse time constants; t_0 is the time when the light was switched on (growth) or off (decay); and A, B, C, and D are the scaling constants. The successful examination of the optoelectronic property makes this composite a promising material in the application of the optoelectronic field. The time constants of growth are 42 s and 465 s for τ_1 and τ_2, respectively. For the decay process, the values are τ_3 = 46 s and τ_4 = 184 s. The high values of time constants are due to the defect states present in the RGO-F8T2 composite.

IV. CONCLUSIONS

In conclusion, the electrical conductivity and photocurrent generation in the RGO-F8T2 composite have been studied. The temperature sensing activity of the composite has also been investigated. The negative temperature coefficient of resistance of the composite is more sensitive compared to the commercially available temperature sensor like Platinum, Polysilicon, and Germanium. The electrical conductivity was explained on the basis of phonon assisted tunneling in between the defect states. The density of states at the Fermi level was observed to increase with an increase in temperature. The absence of scaling in conductivity isotherms was claimed to occur due to the transfer of intramolecular energy from disordered to ordered chain segments or both in the composite. The photocurrent generation in a large area RGO–F8T2 composite film device under simulated solar light illumination has been investigated (Scheme 1). The devices exhibited variation of the photosensitivity with the intensity of incident light. Overall, this work is highly imperative in the field of electrical conduction and photocurrent generation in the RGO based composite for

SCHEME 1. Schematic representation of the synthesis of the RGO-F8T2 composite.

optoelectronic devising used for light energy harvesting and environmental applications.

SUPPLEMENTARY MATERIAL

See the supplementary material for XPS analysis, TCR calculation, variation of impedance, dielectric context, and electrical modulus with frequency.

ACKNOWLEDGMENTS

This work was supported by the Department of Science and Technology (DST), New Delhi, India, through Grant No. SR/FTP/PS-113/2010. We are also thankful to the University Grants Commission (UGC), New Delhi, India, and DST, New Delhi, India, for providing special assistance and infrastructural support to the Department of Physics & Technophysics, Vidyasagar University, through the SAP and FIST program, respectively. We extend our thanks to the Department of Physics and Meteorology, IIT Kharagpur, for providing access to the DST-FIST funded XPS facility.

REFERENCES

[1]A. Dodabalapur, Mater. Today **7**, 56 (2004).
[2]R. F. Service, Science **278**, 383 (1997).
[3]F. Garnier, R. Hajlaoui, A. Yassar, and P. Srivastava, Science **265**, 1684 (1994).
[4]C. J. Drury, C. M. J. Mutsaers, C. M. Hart, M. Matters, and D. M. de Leeuw, Appl. Phys. Lett. **73**, 108 (1998).
[5]H. Sirringhaus, N. Tessler, and R. H. Friend, Science **280**, 1741 (1998).
[6]H. Sirringhaus, Adv. Mater. **26**, 1319 (2014).
[7]R. A. Street and A. Salleo, Appl. Phys. Lett. **81**, 2887 (2002).
[8]H. Sirringhaus, R. J. Wilson, R. H. Friend, M. Inbasekaren, W. Wu, E. P. Woo, M. Grell, and D. D. C. Bradley, Appl. Phys. Lett. **77**, 406 (2000).
[9]P. A. Levermore, R. Jin, X. Wang, J. C. de Mello, and D. D. C. Bradley, Adv. Funct. Mater. **19**, 950 (2009).
[10]H. Sirringhaus, T. Kawase, R. H. Friend, T. Shimoda, M. Inbasekaran, W. Wu, and E. P. Woo, Science **290**, 2123 (2000).
[11]J. Swensen, J. Kanicki, and A. J. Heeger, Proc. SPIE **5217**, 159 (2003).
[12]K. Chakraborty, P. Das, S. Chakrabarty, T. Pal, and S. Ghosh, ChemPhysChem **17**, 1518 (2016).
[13]C. Lampadaris, I. Sakellis, and A. N. Papathanassiou, Appl. Phys. Lett. **110**, 222901 (2017).
[14]G. Wei, J. Yu, M. Gu, and T. B. Tang, J. Appl. Phys. **119**, 224102 (2016).
[15]S. Chakrabarty, K. Chakraborty, A. Laha, T. Pal, and S. Ghosh, J. Phys. Chem. C **118**, 28283 (2014).
[16]K. Chakraborty, T. Pal, and S. Ghosh, ACS Appl. Nano Mater. **1**, 3137 (2018).
[17]K. Chakraborty, S. Chakrabarty, P. Das, S. Ghosh, and T. Pal, Mater. Sci. Eng. B **204**, 8 (2016).
[18]C. Nethravathi and M. Rajamathi, Carbon **46**, 1994 (2008).
[19]J. Jo, D. Vak, Y.-Y. Noh, S.-S. Kim, B. Lim, and D.-Y. Kim, J. Mater. Chem. **18**, 654 (2008).
[20]R. F. Rodrigues, A. Charas, J. Morgado, and A. Maçanita, Macromolecules **43**, 765 (2010).
[21]F. Mailly, A. Giani, R. Bonnot, P. Temple-boyer, F. Pascal-delannoy, A. Foucaran, and A. Boyer, Sens. Actuat. A Phys. **94**, 32 (2001).
[22]A. J. Dekker, *Solid State Physics* (Macmillan, London, 1967).
[23]A. K. Jonscher, Nature **267**, 673 (1977).
[24]N. F. Mott and E. A. Davis, *Electron Processes in Non-crystalline Materials* (Clarendon Press, Oxford, 1979).
[25]M. Pollak and T. H. Geballe, Phys. Rev. **122**, 1742 (1961).
[26]S. Mitra, S. Banerjee, and D. Chakravorty, J. Appl. Phys. **113**, 154314 (2013).
[27]T. Paul and A. Ghosh, J. Appl. Phys. **121**, 135106 (2017).
[28]H. Gargama, A. K. Thakur, and S. K. Chaturvedi, J. Appl. Phys. **117**, 224903 (2015).
[29]S. Ghosh, S. Najmaei, S. Kar, R. Vajtai, J. Lou, N. R. Pradhan, L. Balicas, P. M. Ajayan, and S. Talapatra, Phys. Rev. B **89**, 125422 (2014).
[30]D. P. Almond and A. R. West, Nature **306**, 456 (1983).

[31]S. Ghosh and A. Ghosh, J. Appl. Phys. **97**, 123525 (2005).
[32]T. Paul and A. Ghosh, J. Appl. Phys. **123**, 045107 (2018).
[33]A. R. Long, Adv. Phys. **31**, 553 (1982).
[34]S. R. Elliott, Adv. Phys. **36**, 135 (1987).
[35]H. Böttger and V. V. Bryskin, Phys. Stat. Sol. b **78**, 415 (1976).
[36]L. Kinder, J. Kanicki, J. Swensen, and P. Petroff, Proc. SPIE **5217**, 35 (2003).
[37]R. E. D. Paolo, J. S. de Melo, J. Pina, H. D. Burrows, J. Morgado, and A. L. Maçanita, ChemPhysChem **8**, 2657 (2007).
[38]J–L Brédas, D. Beljonne, V. Coropceanu, and J. Cornil, Chem. Rev. **104**, 4971 (2004).
[39]A. Ghosh and A. Pan, Phys. Rev. Lett. **84**, 2188 (2000).
[40]D. Paria, H–H Jeong, V. Vadakkumbatt, P. Deshpande, P. Fischer, A. Ghosh, and A. Ghosh, Nanoscale **10**, 7685 (2018).
[41]H. Selvi, N. Unsuree, E. Whittaker, M. P. Halsall, E. W. Hill, A. Thomas, P. Parkinson, and T. J. Echtermeyer, Nanoscale **10**, 3399 (2018).
[42]J. Sun, L. Xiao, D. Meng, J. Geng, and Y. Huang, Chem. Commun. **49**, 5538 (2013).
[43]C. Li, Q. Cao, F. Wang, Y. Xiao, Y. Li, J–J Delaunay, and H. Zhu, Chem. Soc. Rev. **47**, 4981 (2018).
[44]X. Fang, P. Wei, L. Wang, X. Wang, B. Chen, Q. He, Q. Yue, J. Zhang, W. Zhao, J. Wang, G. Lu, H. Zhang, W. Huang, X. Huang, and H. Li, ACS Appl. Mater. Interfaces **10**, 13011 (2018).
[45]J. Liu, Q. Huang, K. Zhang, Y. Xu, M. Guo, Y. Qian, Z. Huang, F. Lai, and L. Lin, Nanoscale Res. Lett. **12**, 259 (2017).
[46]P. Das, K. Chakraborty, S. Chakrabarty, S. Ghosh, and T. Pal, Chem. Select **2**, 3297 (2017).
[47]E. J. H. Lee, L. Zhi, M. Burghard, K. Mullen, and K. Kern, Adv. Mater. **22**, 1854 (2010).
[48]K. Chakraborty, S. Chakrabarty, T. Pal, and S. Ghosh, New J. Chem. **41**, 4662 (2017).